2021 43rd Annual International Conference of the
IEEE Engineering in Medicine & Biology Society (EMBC)
Oct 31 - Nov 4, 2021. Virtual Conference

Efficient Artifact Removal from Low-Density Wearable EEG using Artifacts Subspace Reconstruction

Velu Prabhakar Kumaravel*,Victor Kartsch*, Simone Benatti, Giorgio Vallortigara,
Elisabetta Farella, and Marco Buiatti

Abstract— **Light-weight, minimally-obtrusive mobile EEG systems with a small number of electrodes (i.e., low-density) allow for convenient monitoring of the brain activity in out-of-the-lab conditions. However, they pose a higher risk for signal contamination with non-stereotypical artifacts due to hardware limitations and the challenging environment where signals are collected. A promising solution is Artifacts Subspace Reconstruction (ASR), a component-based approach that can automatically remove non-stationary transient-like artifacts in EEG data. Since ASR has only been validated with high-density systems, it is unclear whether it is equally efficient on low-density portable EEG. This paper presents a complete analysis of ASR performance based on clean and contaminated datasets acquired with BioWolf, an Ultra-Low-Power system featuring only eight channels, during SSVEP sessions recorded from six adults. Empirical results show that even with such few channels, ASR efficiently corrects artifacts, enabling an overall enhancement of up to 40% in SSVEP response. Furthermore, by choosing the optimal ASR parameters on a single-subject basis, SSVEP response can be further increased to more than 45%. These results suggest that ASR is a viable and robust method for online automatic artifact correction with low-density BCI systems in real-life scenarios.**

I. INTRODUCTION

Electroencephalography (EEG) is a non-invasive, low-cost technique for investigating brain function and pathology [1]. Thanks to recent technological advances in microprocessor design, wireless communication, and innovative dry electrodes, wearable wireless EEG systems can be implemented to record the brain activity of subjects outside the controlled laboratory settings [2], [3]. This opens a doorway to monitoring EEG data in populations like patients and infants to identify reliable bio-markers of various cognitive disorders.

However, in unconstrained settings, artifacts generated by biological (i.e., eye blinks and movements, motion) and equipment noise are more frequent than in controlled laboratory settings. Thus, removal of such artifacts is crucial to reliably measure brain activity. Moreover, in order to obtain a robust quality measure of the data during EEG acquisition, it should be possible to perform such artifact correction in almost near real-time.

The existing tools for correcting the most common stereotypical artifacts (e.g. eye blinks or movements) [4], [5] generated by adult subjects in controlled settings do not account for non-stereotypical artifacts such as motion, which are prevalent in natural settings and among pediatric populations.

One of the successful algorithms handling this challenge is Artifact Subspace Reconstruction (ASR), an online, automatic, component-based artifact removal method for non-stationary large-amplitude or transient artifacts [6]. While ASR requires no training to identify such artifacts, its performance is highly dependent on the choice of its user-defined parameters. The most crucial one, *ASR Rejection Threshold Parameter* k, was extensively studied in [7], where a value between 20 and 30 is suggested for high-density EEG data. Moreover, as a co-variance-based component method, ASR cannot be applied to single channel EEG. For an effective artifact removal, a standard EEG system with at least 20 channels is recommended [7]. Therefore, it is not yet clear whether ASR could efficiently remove artifacts on data from low-density wearable EEG systems, and if so what could be its optimal parameters.

This work tests ASR performance for automatic removal of both stereotypical and non-stereotypical artifacts from data recorded with a low-density portable EEG system in unconstrained settings. For this purpose, we recorded Steady-State Visual Evoked Potentials (SSVEP), a widely used paradigm to reliably measure sensory and cognitive responses among adults [8], infants [9], and newborns [10], with a portable wireless EEG system based on BioWolf [11] driving 8 electrodes. Specifically, we presented six young adult subjects with a visual stimulation consisting of black and white checkerboard patterns undergoing on-off sinusoidal dynamics at stimulation frequencies ranging from 8 Hz (for which SSVEPs are typically very robust) to 2 Hz (a frequency more appropriate for pediatric studies [9], [10] but more vulnerable to low-frequency artifacts and endogenous fluctuations). Besides providing novel findings about ASR performance with a low-density portable EEG system, to the best of our knowledge, this is the first study to validate ASR on SSVEPs.

To quantify artifact removal against an artifact-free baseline condition, we asked our subjects to stay still and minimize artifacts during half of the experimental sessions (*Artifact-Free* condition) and to deliberately generate motion and eye movement artifacts during the other half of the sessions (*Artifact* condition). We then varied ASR parameters to find the optimal ones for artifact removal. Differently

* These authors contributed equally to this work
The ERC PoC grant NeuroSoNew (842243) to G.V. supported this work.
V.P. Kumaravel and E.Farella are with Fondazione Bruno Kessler, Trento, Italy. (email: {vkumaravel, efarella}@fbk.eu)
V.P. Kumaravel, V. Kartsch, M. Buiatti and G. Vallortigara are with CIMeC, University of Trento, Italy. (email:{velu.kumaravel, vj.kartschmorinigo, marco.buiatti,giorgio.vallortigara} @unitn.it)
S. Benatti is with the University of Bologna, Italy. (email: {simone.benatti} @unibo.it) and also with the Dipartimento di Scienze e Metodi dell'Ingegneria, University of Modena e Reggio Emilia, Italy (email: simone.benatti@unimore.it)

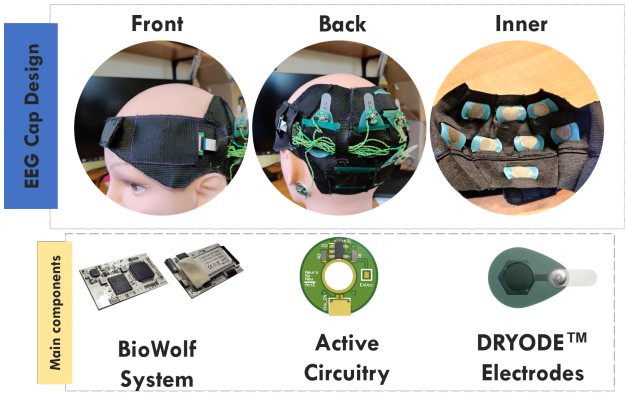

Fig. 1: Portable EEG system embedding BioWolf and eight Dryode™ electrodes featuring active signal buffering.

from previous studies [7], not only we systematically varied ASR key parameter k, but we also compared the two main processing modes of ASR: removing artifacts from bad segments (Correction) or rejecting bad segments (Removal). We tested the ASR performance by comparing SSVEPs of ASR-cleaned data from artifact-free and artifacted sessions at all stimulation frequencies.

II. Materials and Methods

A. BioWolf-based acquisition system

BioWolf is a highly wearable platform for BCIs and medical-grade IoT applications, targeting raw data streaming and on-board digital signal processing [11]. Signal acquisition relies on the ADS1298 from Texas Instruments, a de-facto standard for biopotential acquisition platforms by virtue of its favorable trade-off between signal quality and energy efficiency. The ADS1298 allows simultaneous sampling of up to eight bipolar channels (24 bits) at a maximum sample rate of 32 kbps.

BioWolf integrates two MCUs, namely, an Arm Cortex-M4 SoC from Nordic (nRF52832), serving as wireless transmission device (BLE 5.0) and as the system's general manager, and Mr. Wolf (PULP) [12], an Ultra-Low-Power (ULP) System on Chip (SoC) for real-time and energy-efficient processing of biosignal algorithms. Additionally, BioWolf incorporates an electrode contract quality subsystem, a battery manager (BQ25570), and an IMU device (IIS2DH) to register acceleration and temperature.

For the acquisition of EEG signals, BioWolf is coupled with a custom elastic EEG cap featuring eight dry soft electrodes from Idun Technologies [13]. Each electrode includes an active circuitry [2] based on the AD8603 (Analog Devices), which improves the overall CMRR and minimizes the artifacts due to cable movement. Fig. 1 shows the complete EEG cap implementing all the components introduced above.

B. EEG Acquisition Setup

Six healthy subjects (aged 25-35 years) participated in data collection, performed in a controlled environment (dimmed light, silent, and apart from electrical interference sources). All participants reported no history of neurological or psychiatric disorders and provided written consent to participate in the experiments.

Stimuli consisted of a black and white 10x10 square checkerboard presented on a uniform grey background at a distance of 80 cm from the subject's eyes, subtending a visual angle of approximately 15x15° and based on a sinusoidal on-off 100% contrast temporal modulation. Compared to abrupt on/off dynamics, such sinusoidal modulation reduces the number of harmonics [8] while producing a pleasant and less fatiguing visual stimulation. Additionally, a thin black diagonal cross was overlapped to the checkerboard to help with visual fixation. All textures have been generated with Psychtoolbox 3.0.12 based on Matlab 2020b (MathWorks Inc.) for Windows.

Stimuli were presented in series of three trials of 25 seconds each at three different temporal frequencies (2Hz, 4Hz, 8Hz) in randomized order. The complete testing session contained six series alternating between *Artifact-Free* and *Artifact* conditions. During an *Artifact-Free* session, subjects were asked to relax (hence, minimizing artifacts) while focusing on the stimuli. During an *Artifact* session, subjects actively induced artifacts by changing the seating position, moving their heads and repeatedly blinking, while keeping their attention on the stimuli. They were asked to keep their visual fixation at the center of the checkerboard for all trials.

Before starting the experiments, the acquisition system (battery and triggers) and the electrode contact quality were checked. As the dry electrodes' flat surface only allows for proper skin contact when no hair is present, an electrode gel was used to adjust the contact quality of haired subjects, when required.

Fig. 2: Comparison of average FTR (see section II-E.4) across all subjects without ASR (blue), with ASR and best k for each subject for both ASR Correction (orange), and ASR Removal (green). Error bars show the s.e.m. across subjects.

C. Artifacts Subspace Reconstruction (ASR)

ASR is an automated artifact removal technique to detect/remove transient high-amplitude artifacts in continuous EEG data. It is available as an open-source EEGLAB [14] plug-in function *clean_rawdata* [15]. ASR processes artifacts in four steps which are briefly described as follows (For a more detailed technical documentation refer to [16]):

1) Step 1: ASR Calibration: As a first step, ASR automatically identifies highly contaminated portions of EEG signals based on a predefined robust power distribution estimation. The remaining portions (i.e., cleaner portions) are concatenated together to form the calibrated data.

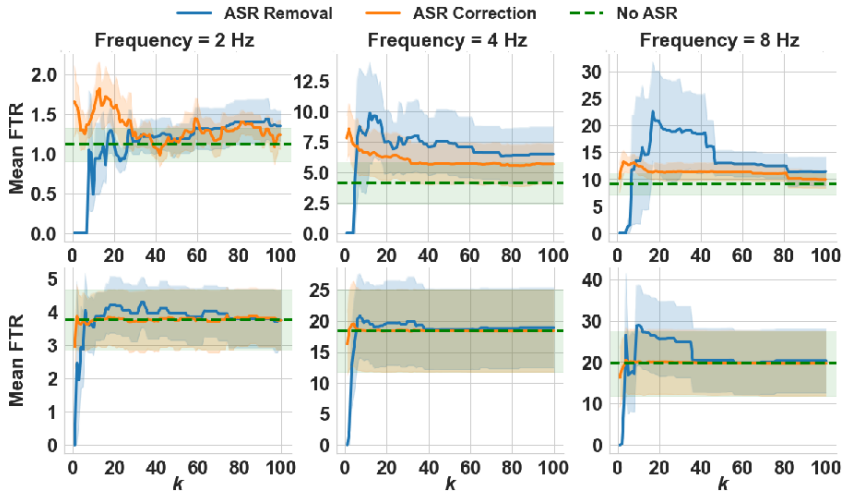

Fig. 3: ASR Performance: FTR metric as a function of ASR parameter k and processing mode for *Artifact* (top panel) and *Artifact-Free* (bottom panel) Conditions.

2) Step 2: Computation of Rejection Threshold: To estimate the rejection criteria, Principal Component Analysis (PCA) is performed on the identified calibrated data and component-wise RMS for each window is computed. For each component i, mean (μ_i) and standard deviation (σ_i) of RMS across all windows is evaluated. ASR then defines rejection thresholds as $T_i = \mu_i + k.\sigma_i$ where k is a user-defined parameter.

3) Step 3: Identification of Artifact Subspace: ASR computes PCA on the original data in a sliding window fashion. The energy of each component for a given window is compared to that obtained from the threshold computed in Step 2. The components that exceed the threshold are labeled as Artifact Subspace.

4) Step 4: Artifact Subspace Processing: In the final step, ASR removes the detected artifact subspace for each window in the Principal Component space. The artifact-corrected EEG is computed by back-projecting the residual non-artifactual components to the original electrode space keeping the original length of the data. This is indicated as *ASR Correction* in this paper.

It is also possible to remove the identified noisy segments, a processing mode hereafter mentioned as *ASR Removal*.

D. Evaluation of ASR Parameters

In this work, the following user-defined parameters are studied, leaving the system parameters with default settings:

1) ASR Processing Mode: As mentioned earlier, ASR can operate in two distinct modes – *ASR Correction* and *ASR Removal*. While *ASR Correction* preserves the length of input data by modifying the detected noisier segments, *ASR Removal* rejects those segments.

2) ASR Rejection Threshold Parameter (k): k is the standard deviation multiplicative factor (Section II-C.2), the key parameter defining artifacts' rejection threshold.

E. EEG Data Analysis

Data analysis was performed with EEGLAB toolbox [17] and custom-made software based on MATLAB R2018b (Natick, MA).

1) Pre-Processing: EEG data were first low-pass filtered with a cut-off frequency of 40 Hz to remove the line and high-frequency noise. Subsequently, a high-pass filter based on *clean_drifts* EEGLAB function [15] (transition band: 0.15-0.3 Hz) was applied to remove low-frequency artifacts.

2) ASR Processing: Bad segments were processed by ASR using the dedicated EEGLAB plug-in [15]. To evaluate the aforementioned user parameters, we processed the data with k values ranging from 1 to 100 for both *ASR Correction* and *ASR Removal* processing modes.

3) Fourier Analysis: For each of the three stimulation frequencies, stimulus-specific trials were extracted, segmented in overlapping epochs of 10s (overlap factor varied between 1/2 and 3/4 of epoch length to adjust to the variable length of clean data segments), and Fourier transform F(f) of each epoch was computed using MATLAB's FFT function. The power spectrum was calculated from these Fourier coefficients as the average over epochs of the single-epoch power spectrum: $PS(f) = \langle F(f) \times F^{*}(f) \rangle_{ep}$

4) Measure of SSVEP Response: To extract a SSVEP normalized measure, we computed the Frequency-Tagged Response (FTR) as the ratio between the power spectrum at the stimulation frequency and the average of the power spectrum over the six neighboring frequency bins (±0.3 Hz)[10]. To test the performance of ASR in recovering a reliable SSVEP response from the *Artifact* sessions, for each subject and stimulation frequency, we selected the electrode with the highest FTR in *Artifact-Free* sessions.

III. Results

A. Artifacts impact SSVEPs

As expected, artifacts severely deteriorate data quality and hamper SSVEP detection. To quantify this, we computed FTR on the band-pass filtered data without ASR processing. As shown in Fig 2 (blue bars), the *Artifact* sessions produced a significantly lower FTR compared to *Artifact-Free* sessions. This effect appears at all three stimulus frequencies. It is worth mentioning that the average FTR for 2 Hz is around 1, which is equivalent to no SSVEP response.

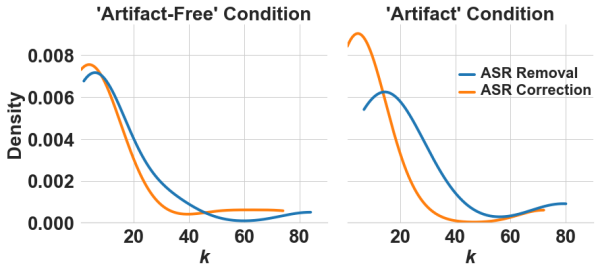

Fig. 4: Distribution of single-subject optimal k values for *Artifact-Free* (left) and *Artifact* (right) conditions across all stimulation frequencies.

B. Overall Performance of ASR

For each stimulus frequency, we identified a range of ASR parameter k and processing mode that remarkably enhanced the FTR for all subjects in *Artifact* condition. Specifically, ASR performance was more successful in *Correction* mode for 2 Hz (18.7% FTR increase), and in *Removal* mode for 4 Hz (67.5% FTR increase) and 8 Hz (49.5% FTR increase).

One possible explanation for this frequency-dependent behaviour is that a 2 Hz SSVEP signal requires a higher number of samples to perform FFT compared to that of a 4 Hz or an 8 Hz signal. With *Removal*, some subjects have not enough samples to compute FFT, leading to an average poor FTR score. However, with higher k-values (>25) leading to a relaxed threshold, *Removal* performs similar to *Correction* as evident in Fig. 3 (blue vs orange).

The best performing k values ranged between 10 and 20 for 2 Hz and 4 Hz, and between 15 and 40 for 8 Hz in their respective best processing mode. It is worth noting that ASR processing also improved the SSVEP response in *Artifact-Free* sessions, especially in *Removal* mode and for 8 Hz [Fig. 3 (bottom panel)].

C. Subject-specific ASR Parameter Optimization

To further investigate the variability of optimal k at the single-subject level, we studied the distribution of k-values that maximized the FTR for each subject and frequency in both processing modes. In line with the state-of-the-art guidelines [7], the distribution of k is concentrated between 1 and 40 in both *Artifact-Free* and *Artifact* conditions (Fig. 4). We also observed that for *Correction* mode, optimal k values range between 1 and 20 for most subjects while for *Removal* mode, the distribution is shifted to higher values starting from k = 8. This suggests that when opting for *Removal* instead of *Correction*, a slightly higher k is recommended to avoid too much data removal hence preserving sufficient data for post-processing.

We then computed the average FTR of all subjects with their respective optimal k-values, for each processing mode. As it can be clearly seen in fig. 2, ASR significantly improved FTR (up to 45%) for all three stimulation frequencies in *Artifact* sessions.

IV. CONCLUSIONS

In this study, we demonstrated that, by choosing appropriate processing parameters, ASR is efficient in removing artifacts and recovering significant SSVEP responses at multiple stimulation frequencies from low-density EEG data recorded by a portable ultra-low-power system. Additionally, we found that ASR performance is highly dependent on its k parameter and processing mode (correction/removal), such that a poor choice might lead to a potential degradation in signal quality. Therefore, it is recommended to first establish the optimal k and processing mode on similar EEG data from the same EEG system (i.e., training data).

We conclude that ASR is a reliable artifact processing technique in low-density, potentially real-time BCI systems that can be used to measure neural response in diverse applications as real-life settings and/or among clinical and pediatric populations.

REFERENCES

[1] E. Niedermeyer and F. L. da Silva, *Electroencephalography: Basic Principles, Clinical Applications, and Related Fields*. Lippincott Williams & Wilkins, 2005.

[2] M. Guermandi, R. Cardu, E. F. Scarselli, and R. Guerrieri, "Active electrode ic for eeg and electrical impedance tomography with continuous monitoring of contact impedance," *IEEE transactions on biomedical circuits and systems*, vol. 9, no. 1, pp. 21–33, 2015.

[3] V. Kartsch, M. Guermandi, S. Benatti, F. Montagna, and L. Benini, "An energy-efficient iot node for hmi applications based on an ultra-low power multicore processor," in *2019 IEEE Sensors Applications Symposium (SAS)*. IEEE, 2019, pp. 1–6.

[4] A. Mognon, J. Jovicich, L. Bruzzone, and M. Buiatti, "Adjust: An automatic eeg artifact detector based on the joint use of spatial and temporal features," *Psychophysiology*, vol. 48:2, p. 229–40, Jan 2011.

[5] L. Pion-Tonachini, K. Kreutz-Delgado, and S. Makeig, "Iclabel: An automated electroencephalographic independent component classifier, dataset, and website," *NeuroImage*, vol. 198, pp. 181–197, 2019.

[6] T. R. Mullen, C. A. E. Kothe, Y. M. Chi, A. Ojeda, T. Kerth, S. Makeig, T. Jung, and G. Cauwenberghs, "Real-time neuroimaging and cognitive monitoring using wearable dry eeg," *IEEE Transactions on Biomedical Engineering*, vol. 62, no. 11, pp. 2553–2567, 2015.

[7] C. Y. Chang, S. H. Hsu, L. Pion-Tonachini, and T. P. Jung, "Evaluation of artifact subspace reconstruction for automatic artifact components removal in multi-channel eeg recordings," *IEEE Transactions on Biomedical Engineering*, vol. 67, no. 4, pp. 1114–1121, 2020.

[8] A. M. Norcia, L. G. Appelbaum, J. M. Ales, B. R. Cottereau, and B. Rossion, "The steady-state visual evoked potential in vision research: A review," *Journal of vision*, vol. 15, no. 6, pp. 4–4, 2015.

[9] A. De Heering and B. Rossion, "Rapid categorization of natural face images in the infant right hemisphere," *Elife*, vol. 4, p. e06564, 2015.

[10] M. Buiatti, E. Di Giorgio, M. Piazza, C. Polloni, G. Menna, F. Taddei, E. Baldo, and G. Vallortigara, "Cortical route for facelike pattern processing in human newborns," *Proceedings of the National Academy of Sciences*, vol. 116, no. 10, pp. 4625–4630, 2019.

[11] V. Kartsch, G. Tagliavini, M. Guermandi, S. Benatti, D. Rossi, and L. Benini, "Biowolf: A sub-10-mw 8-channel advanced brain–computer interface platform with a nine-core processor and ble connectivity," *IEEE transactions on biomedical circuits and systems*, vol. 13, no. 5, pp. 893–906, 2019.

[12] A. Pullini, D. Rossi, I. Loi, A. D. Mauro, and L. Benini, "Mr. wolf: A 1 gflop/s energy-proportional parallel ultra low power soc for iot edge processing," in *ESSCIRC 2018 - IEEE 44th European Solid State Circuits Conference (ESSCIRC)*, Sept 2018, pp. 274–277.

[13] DRYODE^{TM} - IDUN Technologies, https:https://dryode.tech/, 2016.

[14] A. Delorme and S. Makeig, "EEGLAB: an open source toolbox for analysis of single-trial EEG dynamics including independent component analysis," *Journal of Neuroscience Methods*, vol. 134, no. 1, pp. 9–21, Mar. 2004.

[15] "Eeglab plugin: clean_rawdata, https://github.com/sccn/clean_rawdata."

[16] C. A. E. Kothe and T.-P. Jung, "Artifact removal techniques with signal reconstruction," *US. Patent*, vol. 895, p. 440, 2014.

[17] A. Delorme and S. Makeig, "Eeglab: an open source toolbox for analysis of single-trial eeg dynamics including independent component analysis," *Journal of neuroscience methods*, vol. 134, no. 1, p. 9—21, March 2004.